

Mott Transition and Superconductivity in Quantum Spin Liquid Candidate NaYbSe₂

Yating Jia^{1,2,#}, Chunsheng Gong^{3,#}, Yixuan Liu³, Jianfa Zhao¹, Cheng Dong⁴,
Guangyang Dai¹, Xiaodong Li⁵, Hechang Lei^{3,*}, Runze Yu^{1,*}, Guangming Zhang^{6,7}
and Changqing Jin^{1,2*}

¹Institute of Physics, Chinese Academy of Sciences, Beijing 100190, China

²University of Chinese Academy of Sciences, Beijing 100190, China

³Department of Physics and Beijing Key Laboratory of Opto-electronic Functional Materials &
Micro-nano Devices, Renmin University of China, Beijing 100872, China

⁴Peking University Shenzhen graduate School, School of Advanced Materials, Shenzhen 518055,
China

⁵Beijing Synchrotron Radiation Facility, Institute of High Energy Physics, Chinese Academy of
Sciences, Beijing, 100049, China

⁶State Key Laboratory of Low-Dimensional Quantum Physics and Department of Physics,
Tsinghua University, Beijing 100084, China

⁷Frontier Science Center for Quantum Information, Beijing 100084, China

*Corresponding authors: hlei@ruc.edu.cn; yurz@iphy.ac.cn; jin@iphy.ac.cn

#These authors contribute equally to this work.

Abstract:

The Mott transition is one of the fundamental issues in condensed matter physics, especially in the system with antiferromagnetic long-range order. However the Mott transition in quantum spin liquid (QSL) systems without long-range order is rare. Here we report the observation of the pressure-induced insulator to metal transition followed by the emergence of superconductivity in the QSL candidate NaYbSe₂ with triangular lattice of $4f$ Yb³⁺ ions. Detail analysis of transport properties at metallic state shows an evolution from non-Fermi liquid to Fermi liquid behavior when approaching the vicinity of superconductivity. An irreversible structure phase transition occurs around 11 GPa is revealed by the X-ray diffraction and Raman spectrum. These results shed light on the Mott transition and superconductivity in the QSL systems.

Introduction

Frustrated magnets are materials in which localized magnetic moments (spins), interact through competing exchange interactions that cannot be simultaneously satisfied. Magnetic frustration systems have attracted tremendous interests because they exhibit numerous exotic emergent phenomena [1]. One of important examples is quantum spin liquid (QSL) with a ground state of strong quantum fluctuations preventing the phase transition towards conventional magnetic order. It exhibits long-range quantum entanglement [1-3] and de-confined spinon excitations that may obey varied statistics rules of boson, fermion, or even anyon depending on the types of QSL [2]. More importantly, Anderson proposed that the superconductivity in copper oxide superconductors can evolve from spin liquid state [4]. Therefore, Mott transition and superconductivity emerging from the QSL are very interesting.

Mott transition is one of the important subjects in the physics of strongly correlated electrons especially in the system with antiferromagnetic long-range order [5]. However the ground state of the Mott insulator in QSLs is not trivial and Mott transition between metallic and insulating spin-liquid phase is very rare [1]. For example attempt to dope QSL candidate $\text{ZnCu}_3(\text{OH})_6\text{C}_{12}$ indicated there was no observation for metallic or superconducting states even up to 0.6 electron per Cu^{2+} and down to 1.8 K [6]. Theoretical analysis found the localization of electrons in various Zn-Cu hydroxyl halides and the formation of polaronic states with attendant lattice displacements and a dramatic narrowing of bandwidth upon electron addition [7]. Compare with charge carriers doping, pressure is an effective and clean approach to induce Mott transition. For example, pressure-induced (band-width-controlled) metal-insulator transition (MIT) with exotic quantum criticality and superconductivity appears in the vicinity of MIT with possible unconventional mechanisms in organic QSL candidates $\kappa\text{-(ET)}_2\text{Cu}_2(\text{CN})_3$ and $\kappa\text{-(ET)}_2\text{Ag}_2(\text{CN})_3$ [8-14], in which the Hubbard U is relative small. In contrast, although external pressure can modify magnetic properties of quasi-two-dimensional (quasi-2D) inorganic frustrated systems significantly by way of tuning magnetic exchange interaction, crystal energy field (CEF), dipole interaction [15], the insulating

behavior still persists under high pressure, such as in α -RuCl₃ and α -Li₂IrO₃ [16, 17, 18], possibly due to the large U in these strong Mott insulators. Takagi *et al.* claimed the observation of the pressure induced insulating to metallic phase transition in QSL candidate Na₄Ir₃O₈ [19], but there was no report on the details of experiment. Thus, the MIT in quasi-2D inorganic magnetic frustrated inorganic materials is still elusive.

Very recently, a novel material system NaLnCh₂ (Ln = rare earth, Ch = O, S, Se), especially NaYbCh₂, has been proposed to be a promising candidate to realize QSL state [20-23]. NaYbCh₂ has a perfect triangle lattice and similar CEF environment of 4fYb³⁺ ions to YbMgGaO₄ [24]. Thus NaYbS₂ is an effective spin-1/2 quantum magnet at low temperature. It possesses the simplest structure and chemical formula among the known QSL candidates. In addition, the antiferromagnetic exchange interaction is significantly enhanced ($|\theta_{CW}| > 10$ K) [20-22], and the site disorder of elements is absent in NaYbCh₂ compared to YbMgGaO₄. Importantly, the long-range magnetic order or spin glass states are not observed in NaYbCh₂ when temperature down to 50 mK, generating an empirical frustration parameter $f = \theta_{CW}/T_N > 200$ [20-23]. Continuous magnetic excitations are also observed in NaYbO₂ by inelastic neutron scattering show a gapless feature [23]. These results strongly suggest that NaYbCh₂ with strong spin-orbital coupling (SOC) could host a QSL state as the ground state. Moreover the absorption spectra indicate that the charge gaps are roughly 4.5 eV, 2.7 eV and 1.9 eV for NaYbO₂, NaYbS₂ and NaYbSe₂, respectively. The variable and small charge gaps may allow the system to access a MIT by applying pressures.

In this work, we study the pressure effects on structural and transport properties of NaYbSe₂ up to 125.9 GPa. It is found that there is a structural transition from the $R\bar{3}mH$ to $P\bar{3}m1$ at around 11 GPa. A MIT appears at about 58.9 GPa, accompanying with the giant change of resistivity by 8 orders of magnitude. A superconducting transition emerges when pressure is higher than 103.4 GPa.

Experimental

Single crystals of NaYbSe₂ were grown by NaCl flux method. The mixture of Yb powder, Se grain and NaCl grain with the molar ratio of 2 : 3 : 10 was loaded into a

silica tube and then sealed under Ar atmosphere (~ 0.2 atm). The sealed tube was heated to 1173 - 1223 K for 24 h and kept at that temperature for 150 h. Then it was cooled down to room temperature naturally. Finally, the single crystals were separated by washing NaCl flux with distilled water for several times. NaYbSe₂ powders were synthesized by solid state reaction method as described in elsewhere [20].

The electronic transport properties of NaYbSe₂ under high pressure and low temperatures were investigated via four-probe electrical conductivity method in a diamond anvil cell (DAC) made of CuBe alloy as described in references [25-29]. Pressure was generated by a pair of diamonds with a 100 μm diameter culet. A gasket made of T301 stainless steel was pressed from a thickness of 250 μm to 20 μm , and drilled a center hole with a diameter of 300 μm . Fine cubic boron nitride (cBN) powder was used to cover the gasket to protect the electrode leads insulated from the metallic gasket. The electrodes were slim Au wires with a diameter of 18 μm . A 50 μm -diameter center hole in the insulating layer was used as the sample chamber. The dimension of the sample was about 45 $\mu\text{m} \times 45 \mu\text{m} \times 5 \mu\text{m}$, and NaCl powder was as the pressure transmitting medium. The pressure was measured via the ruby fluorescence method at room temperature before and after each cooling [30]. The diamond anvil cell was placed inside a MagLab system to perform the experiments. The temperature was automatically controlled by a program of the MagLab system. A thermometer was mounted near the diamond in the diamond anvil cell to monitor the exact sample temperature.

In-situ high pressure angle-dispersive X-ray diffraction (ADXRD) experiments were performed using a symmetric Mao Bell DAC at Beijing Synchrotron Radiation Facility. The wavelength is 0.6199 Å. The sample in DAC is fine NaYbSe₂ powder and a tiny ruby chip was regarded as the pressure marker. The two dimensional image plate patterns obtained were converted to one-dimensional 2θ versus intensity data using the Fit2d software package [31]. Raman spectra measurement was performed using the Renishaw micro-Raman spectrometer with a symmetric Mao-Bell DAC at room temperature. The wavelength of laser is 532 nm.

Results and discussion

Figure 1(a) shows the evolution of in-plane resistance $R(T)$ as a function of temperature for NaYbSe₂ single crystal at various pressures below 49.6 GPa. Before 8 GPa, we can't measure the $R(T)$ curve via four-probe method because of high resistance of NaYbSe₂. All of $R(T)$ curves show an insulating behavior that increases with decreasing temperature, but the absolute values of $R(T)$ at room temperature decrease with increasing pressure dramatically by more than eight orders of magnitude. The transport behavior can be fitted well by using a variable range hopping model $R(T) = R_0 \exp(T_0/T)^{1/(d+1)}$, where T_0 is the characteristic temperature and $d = 2$ for the two dimensional system. This formula is usually used to describe the weak conducting behavior of Mott insulator. The inset of Fig. 1(b) shows the fitting result of $R(T)$ at $P = 42$ GPa and the fitted T_0 is shown in the main panel of Fig. 1(b). It can be seen that the T_0 decreases gradually with pressure, i.e., the hopping barrier or band gap decreases under pressure. When increasing pressure further ($P = 58.9$ GPa), a metallic state is observed (Fig. 1(c)), but with a minimum around 55 K (Defined as T_{\min}). Carefully checking the resistance below T_{\min} , we find that it obeys a logarithmic temperature dependence (Inset of Fig. 1(c)), which may be explained by either weak localization effect originated from the presence of disorder potentials or incoherent Kondo effect due to the presence of quantum magnetic impurities [32]. Considering that the electric resistivity of the samples in the paramagnetic insulating phase is fitted to the variable range hopping model, we tend to interpret the resistivity up-turn at low temperatures as the weak localization effect. This minimum shifts progressively to lower temperature under higher pressure, which is similar with that observed in Yb-series heavy-fermion compounds [33], and finally a complete metallic behavior in the whole temperature range (2 - 300 K) is achieved at $P_c = 74.8$ GPa. The piezochromism of the NaYbSe₂ single crystal also reflects the narrowing of hopping barrier or band gap (Fig. 1(d)). The color of sample at low pressure is brown-red, which is coincided with the result reported in previous work [20]. It becomes much darker with the increase of pressure, and only a small amount of red color can be seen on the edge at $P = 37.5$ GPa, indicating the

gradually decrease of hopping barrier or band gap [34]. Finally the sample become completely dark when P is above 42.2 GPa, meaning that the band gap is very small and the light can't go through sample.

Under higher pressure, the values of $R(T)$ continuously decreases with metallic behaviors as shown in Fig. 2(a). Surprisingly, when $P = 103.4$ GPa, a sudden drop at $T \sim 8$ K on the $R(T)$ curve appears, suggesting the emergence of superconductivity (Fig. 2(b)). Although the superconducting transition temperature T_c is almost unchanged with pressure, the resistance drop becomes more obvious (inset of Fig. 2(b)). In addition, with increasing magnetic field along the c axis, the resistance drop at $P = 125.9$ GPa is suppressed gradually (Fig. 2(c)), confirming the drop on $R(T)$ curve at around 8 K originates from the superconducting transition indeed. This result is not identical with any results of pressure induced superconductivity for the single element or binary of Na-Yb-Se. So we can also rule out the possibility from impurities. It is noted that the $R(T)$ does not become zero at 125.9 GPa, which is the maximum pressure can be reached at present experiment condition. This could be induced by the imperfect sample quality or pressure inhomogeneity [35].

In order to analyze the metallic state under pressure, we have applied the power-law fitting $R(T) = R_0 + AT^n$ to the resistance of NaYbSe₂ when $P \geq 74.8$ GPa. The inset of Fig. 2(d) shows the fitting result of $R(T)$ between 8 K and 100 K at 74.8 GPa. It can be seen that the power-law formula fits the experimental data well for the temperature between 8 K and 100 K. The pressure dependence of the exponent n is plotted in Fig. 2(d). At the boundary of MIT, the metallic state of NaYbSe₂ clearly shows a non-Fermi-liquid (NFL) behavior with $n \sim 1$. With increasing pressure, the n increases gradually and finally becomes close to 2 ($n = 2.1(1)$ at $P = 125.9$ GPa), implying the emergence of Fermi-liquid (FL) behavior in NaYbSe₂. Therefore there is a crossover from NFL to FL behavior with increase of pressure when approaching the boundary of superconductivity. Usually, the value of n less than 2 is argued to be caused by quantum critical fluctuations. This phenomena have been observed frequently in heavy-fermion systems where magnetic orders are suppressed by doping, magnetic field or pressure

[36-39]. But it has to be mentioned that the NFL behavior observed in NaYbSe₂ is not confined to the vicinity of P_c , but extends to much higher pressures. More importantly, different from the situation in κ -(ET)₂Cu₂(CN)₃ and κ -(ET)₂Ag₂(CN)₃ that superconductivity usually emerges in the quantum-critical-fluctuation region near the end point of a MIT [8, 9, 14, 39], the superconductivity in NaYbSe₂ seems to appear when P is away from the P_c of MIT and the metallic state exhibits a FL behavior. Such interesting features need to be studied at even higher pressure in the future in order to check whether the value of n is still near 2 in the bulk superconducting region.

Figure 3(a) shows the synchrotron X-ray diffraction patterns under various pressure. At ambient pressure, the pattern can be indexed very well with a space group $R\text{-}3mH$ as reported in the previous work (named phase I) [20]. The peaks shift to the high angle with the increasing of pressure, indicating the shrink of the lattice parameters. The additional peaks around 18.6 degree appear (See arrow in Fig. 3(a)) at around 12 GPa. Finally it completely transferred into a new phase (named phase II) at around 19.4 GPa. The phase II keeps stable with pressure up to 43.5 GPa. When the pressure is released, the high pressure phase can be kept, indicating that the phase transition is irreversible. The structure transition is also confirmed by the micro-Raman spectrum under pressure (Fig. S1). Carefully checking the X-ray diffraction patterns under pressure, it can be seen almost all the patterns at low pressure phase persist to the high pressure phase. For example the peak at around 5.1 degree at ambient pressure (the peak of (003) in phase I), which describes the framework of this hexagonal structure along c axis, keeps alive up to the highest pressure in the experiment, indicating the framework of the low pressure phase is kept at high pressure, and there should be the relative change for the atoms during the phase transition.

After carefully checking the pattern at high pressure we find the high pressure phase pattern can be reproduced with a structure with space group $P\text{-}3m1$. The details of crystal structure refinement and data can be found in Fig. S2 and Table S1. The crystal structures viewed along c axis and ab plane for phase I and II are shown in Figs. 3(b) and (c). Both structures show same hexagonal lattice structure along c axis (See Fig. 3(b)). While the Na and Se layers are pushed to approach to each other under high

pressure in the ab plane compared with the lower pressure phase. In the high pressure phase, two different types of YbSe_6 octahedra stack separately along c axis. The relative movement between Na and Se layers induces the elongation YbSe_6 octahedra along c axis, but it does not change the perfect triangular network of Yb ions. Thus, the features of in-plane magnetic frustration should be still intact for the high pressure phase.

Figure 4 exhibits a pressure-temperature phase diagram of NaYbSe_2 single crystal. As can be seen clearly, the application of high pressure reduces the resistance continuously and a metallic state at 58.9 GPa with a weak localization at low temperature. Then superconductivity appears at 103.4 GPa. There is non-Fermi liquid to Fermi liquid state transition at metallic areas. Meanwhile according to the results of ADXRD and Raman spectroscopy, a structural phase from low pressure phase $R-3mH$ to a high pressure phase with $P-3m1$ occurs. The pressure turned Mott transition and superconductivity is observed at the second phase. Such $P-T$ phase is different from that observed in organic QSL compound $\kappa\text{-(ET)}_2\text{Cu}_2(\text{CN})_3$ [14], in which superconductivity emerges from the quantum-critical-fluctuation region near the end point of a MIT, indicating there may be two different mechanisms for the electronic states evolution in these two system.

Conclusion

In summary, we have discovered pressure-induced MIT at 58.9 GPa and superconductivity appearing at much higher pressure away from MIT ($P = 103.4$ GPa) in QSL candidates NaYbSe_2 , accompanying a structural phase transition around 11 GPa from the $R-3mH$ to $P-3m1$. The low temperature $R(T)$ at metallic state exhibits a crossover from NFL to FL behavior. These observations open up a promising way to study the features of MIT and the interplay between spin and charge degrees of freedom in the QSL system with strong SOC. Furthermore, a large family of NaLnCh_2 compounds provides a novel platform to investigate the effects of $4f$ and chalcogen ions on the possible MIT and superconductivity in magnetic frustration systems.

This work was support by the National Key R&D Program of China, the National

Natural Science Foundation of China, the Fundamental Research Funds for the Central Universities, and the Research Funds of Renmin University of China (RUC).

References

- [1] L. Balents, Spin liquids in frustrated magnets, *Nature* **464**, 199 (2010).
- [2] L. Savary and L. Balents, Quantum spin liquids: a review, *Rep. Prog. Phys.* **80**, 016502 (2017).
- [3] Y. Zhou, K. Kanoda and T. K. Ng, Quantum spin liquid states, *Rev. Mod. Phys.* **89**, 025003 (2017).
- [4] P. W. Anderson, The resonating valence bond state in La_2CuO_4 and superconductivity, *Science* **235**, 1196 (1987).
- [5] M. Imada, A. Fujimori and Y. Tokura, Metal-insulator transitions. *Rev. Mod. Phys.* **70**, 1039 (1998).
- [6] Z. A. Kelly, M. J. Gallagher and T. M. McQueen, Electron doping a Kagome spin liquid, *Phys. Rev. X* **6**, 041007 (2016).
- [7] Q. Liu, G. M. Dalpian and A. Zunger, Antidoping in insulators and semiconductors having intermediate bands with trapped carriers, *Phys. Rev. Lett.* **122**, 106403 (2019).
- [8] H. Ito, T. Ishiguro, M. Kubota and G. Saito, Metal-nonmetal transition and superconductivity localization in the two-dimensional conductor κ -(BEDT-TTF) $_2$ Cu[N(CN) $_2$]Cl under pressure, *J. Phys. Soc. Jpn.* **65**, 2987 (1996).
- [9] Y. Kurosaki, Y. Shimizu, K. Miyagawa, K. Kanoda and G. Saito, Mott transition from a spin liquid to a Fermi liquid in the spin-frustrated organic conductor κ -(ET) $_2$ Cu $_2$ (CN) $_3$, *Phys. Rev. Lett.* **95**, 177001 (2005).
- [10] V. Galitski and Y. B. Kim, Spin-triplet pairing instability of the spinon Fermi surface in a U(1) spin liquid, *Phys. Rev. Lett.* **99**, 266403 (2007).
- [11] Y. Qi and S. Sachdev, Insulator-metal transition on the triangular lattice, *Phys. Rev. B* **77**, 165112 (2008).
- [12] B. J. Powell and R. H. McKenzie, Quantum frustration in organic Mott insulators: from spin liquids to unconventional superconductors, *Rep. Prog. Phys.* **74** 056501 (2011).
- [13] K. Kanoda and R. Kato, Mott physics in organic conductors with triangular lattices, *Annu. Rev. Condens. Matter Phys.* **2**, 167 (2011).
- [14] Y. Shimizu, T. Hiramatsu, M. Maesato, A. Otsuka, H. Yamochi, A. Ono, M. Itoh, M. Yoshida, M. Takigawa, Y. Yoshida and G. Saito, Pressure-tuned exchange coupling of a quantum spin liquid in the

- molecular triangular Lattice κ -(ET)₂Ag₂(CN)₃, Phys. Rev. Lett. **117**, 107203 (2016).
- [15] D. P. Kozlenko, A. F. Kusmartseva, E. V. Lukin, D. A. Keen, W. G. Marshall, M. A. de Vries and K. V. Kamenev, From quantum disorder to magnetic order in an $s = 1/2$ Kagome lattice: a structural and magnetic study of Herbertsmithite at high pressure, Phys. Rev. Lett. **108**, 187207 (2012).
- [16] G. Bastien, G. Garbarino, R. Yadav, F. J. Martinez-Casado, R. Beltrán Rodríguez, Q. Stahl, M. Kusch, S. P. Limandri, R. Ray, P. Lampen-Kelley, D. G. Mandrus, S. E. Nagler, M. Roslova, A. Isaeva, T. Doert, L. Hozoi, A. U. B. Wolter, B. Büchner, J. Geck and J. van den Brink, Pressure-induced dimerization and valence bond crystal formation in the Kitaev-Heisenberg magnet α -RuCl₃, Phys. Rev. B **97**, 241108 (2018).
- [17] J. P. Clancy, H. Gretarsson, J. A. Sears, Y. Singh, S. Desgreniers, K. Mehlawat, S. Layek, G. Kh. Rozenberg, Y. Ding, M. H. Upton, D. Casa, N. Chen, J. Im, Y. Lee, R. Yadav, L. Hozoi, D. Efremov, J. van den Brink and Y. J. Kim, Pressure-driven collapse of the relativistic electronic ground state in a honeycomb iridate, npj Quan. Mater. **3**, 35 (2018).
- [18] Z. Wang, J. Guo, F. F. Tafti, A. Hegg, S. Sen, V. A. Sidorov, L. Wang, S. Cai, W. Yi, Y. Zhou, H. Wang, S. Zhang, K. Yang, A. Li, X. Li, Y. Li, J. Liu, Y. Shi, W. Ku, Q. Wu, R. J. Cava and L. Sun, Pressure-induced melting of magnetic order and emergence of a new quantum state in α -RuCl₃, Phys. Rev. B **97**, 245149 (2018).
- [19] D. Podolsky, A. Paramekanti, Y. Kim and T. Senthil, Mott transition between a spin-liquid insulator and a metal in three dimensions, Phys. Rev. Lett. **102**, 186401 (2009).
- [20] W. Liu, Z. Zhang, J. Ji, Y. Liu, J. Li, X. Wang, H. Lei, G. Chen and Q. Zhang, Rare-earth chalcogenides: a large family of triangular lattice spin liquid candidates, Chin. Phys. Lett. **35**, 117501 (2018).
- [21] M. Baenitz, P. Schlender, J. Sichelschmidt, Y. Onykiienko, Z. Zangeneh, K. Ranjith, R. Sarkar, L. Hozoi, H. Walker, J. Orain, H. Yasuoka, J. van den Brink, H. Klauss, D. Inosov and T. Doert, NaYbS₂: a planar spin-1/2 triangular-lattice magnet and putative spin liquid, Phys. Rev. B **98**, 220409 (2018).
- [22] M. Bordelon, E. Kenney, C. Liu, T. Hogan, L. Posthuma, M. Kavand, Y. Lyu, M. Sherwin, N. Butch, C. Brown, M. Graf, L. Balents and S. Wilson, Field-tunable quantum disordered ground state in the triangular-lattice antiferromagnet NaYbO₂, Nat. Phys. **15**, 1058 (2019).
- [23] L. Ding, P. Manuel, S. Bachus, F. Größler, P. Gegenwart, J. Singleton, R. Johnson, H. Walker, D. Adroja, A. Hillier and A. Tsirlin, Gapless spin-liquid state in the structurally disorder-free triangular

- antiferromagnet NaYbO₂, Phys. Rev. B **100**, 144432 (2019).
- [24] Y. S. Li, H. J. Liao, Z. Zhang, S. Y. Li, F. Jin, L. S. Ling, L. Zhang, Y. M. Zou, L. Pi, Z. R. Yang, J. F. Wang, Z. H. Wu and Q. M. Zhang, Gapless quantum spin liquid ground state in the two dimensional spin-1/2 triangular antiferromagnet YbMgGaO₄, Sci. Rep. **5**, 16419 (2015).
- [25] J. L. Zhang, S. J. Zhang, H. M. Weng, W. Zhang, L. X. Yang, Q. Q. Liu, S. M. Feng, X. C. Wang, R. C. Yu, L. Z. Cao, L. Wang, W. G. Yang, H. Z. Liu, W. Y. Zhao, S. C. Zhang, X. Dai, Z. Fang and C. Q. Jin, Pressure-induced superconductivity in topological parent compound Bi₂Te₃, Proc. Natl. Acad. Sci. **108**, 24 (2011).
- [26] S. J. Zhang, J. L. Zhang, X. H. Yu, J. Zhu, P. P. Kong, S. M. Feng, Q. Q. Liu, L. X. Yang, X. C. Wang, L. Z. Cao, W. G. Yang, L. Wang, H. K. Mao, Y. S. Zhao, H. Z. Liu, X. Dai, Z. Fang, S. C. Zhang and C. Q. Jin, The comprehensive phase evolution for Bi₂Te₃ topological compound as function of pressure, J. Appl. Phys. **111**, 112630 (2012).
- [27] P. P. Kong, F. Sun, L. Y. Xing, J. Zhu, S. J. Zhang, W. M. Li, Q. Q. Liu, X. C. Wang, S. M. Feng, X. H. Yu, J. L. Zhu, R. C. Yu, W. G. Yang, G. Y. Shen, Y. S. Zhao, R. Ahuja, H. K. Mao and C. Q. Jin, Superconductivity in strong spin orbital coupling compound Sb₂Se₃, Sci. Rep. **4**, 6679 (2015).
- [28] J. Zhu, J. L. Zhang, P. P. Kong, S. J. Zhang, X. H. Yu, J. L. Zhu, Q. Q. Liu, X. Li, R. C. Yu, R. Ahuja, W. G. Yang, G. Y. Shen, H. K. Mao, H. M. Weng, X. Dai, Z. Fang, Y. S. Zhao and C. Q. Jin, Superconductivity in topological Insulator Sb₂Te₃ induced by pressure, Sci. Rep. **3**, 2016 (2013).
- [29] L. He, Y. T. Jia, S. J. Zhang, X. Hong, C. Q. Jin and S. Y. Li, Pressure-induced superconductivity in the three-dimensional topological Dirac semimetal Cd₃As₂, npj Quan. Mater. **1**, 16014 (2016).
- [30] H. K. Mao, J. Xu and P. M. Bell, Calibration of the ruby pressure scale to 800-kbar under quasi-hydrostatic conditions, J. Geophys. Res. **91**, 4673 (1986).
- [31] A. P. Hammersley, S. O. Svensson, M. Hanfland, A. N. Fitch and D. Hausermann, Two-dimensional detector software: from real detector to idealized image or two-theta scan, High. Pres. Res. **14**, 235 (1996).
- [32] J. Kondo, Resistance minimum in dilute magnetic alloys, Progress of Theoretical Physics **32**, 37 (1964).
- [33] A. Goltsev and M. Abd-Elmeguid, Origin of the pressure dependence of the Kondo temperature in Ce- and Yb-based heavy-fermion compounds, J. Phys.: Condens. Matter **17**, 813 (2005).
- [34] J. A. Barreda-Argüeso, L. Nataf, F. Aguado, I. Hernández, J. González, A. Otero-de-la-Roza, V. Luaña, Y. T. Jia, C. Q. Jin, B. J. Kim, K. Kim, B. I. Min, W. Heribert, A. P. Jephcoat and F. Rodríguez,

Pressure-induced spin transition and site-selective metallization in CoCl_2 , *Sci. Rep.* **9**, 5548 (2019).

[35] J. G. Cheng, K. Matsubayashi, W. Wu, J. P. Sun, F. K. Lin, J. L. Luo and Y. Uwatoko, Pressure induced superconductivity on the border of magnetic order in MnP, *Phys. Rev. Lett.* **114**, 117001 (2015).

[36] J. Custers, P. Gegenwart, H. Wilhelm, K. Neumaler, Y. Toklwa, O. Trovarelli, G. Geibel, F. Steglich, C. Pepin and P. Coleman, The break-up of heavy electrons at a quantum critical point, *Nature* **424**, 524 (2003).

[37] N. Mathur, F. Grosche, S. Julian, I. Walker, D. Freye, R. Haselwimmer and G. Lonzarich, Magnetically mediated superconductivity in heavy fermion compounds, *Nature* **394**, 39 (1998).

[38] G. R. Stewart, Non-Fermi-liquid behavior in d and f electron metals, *Rev. Mod. Phys.* **73**, 797 (2001).

[39] B. Kyung and A. Tremblay, Mott transition, antiferromagnetism, and d-wave superconductivity in two-dimensional organic conductors, *Phys. Rev. Lett.* **97**, 046402 (2006).

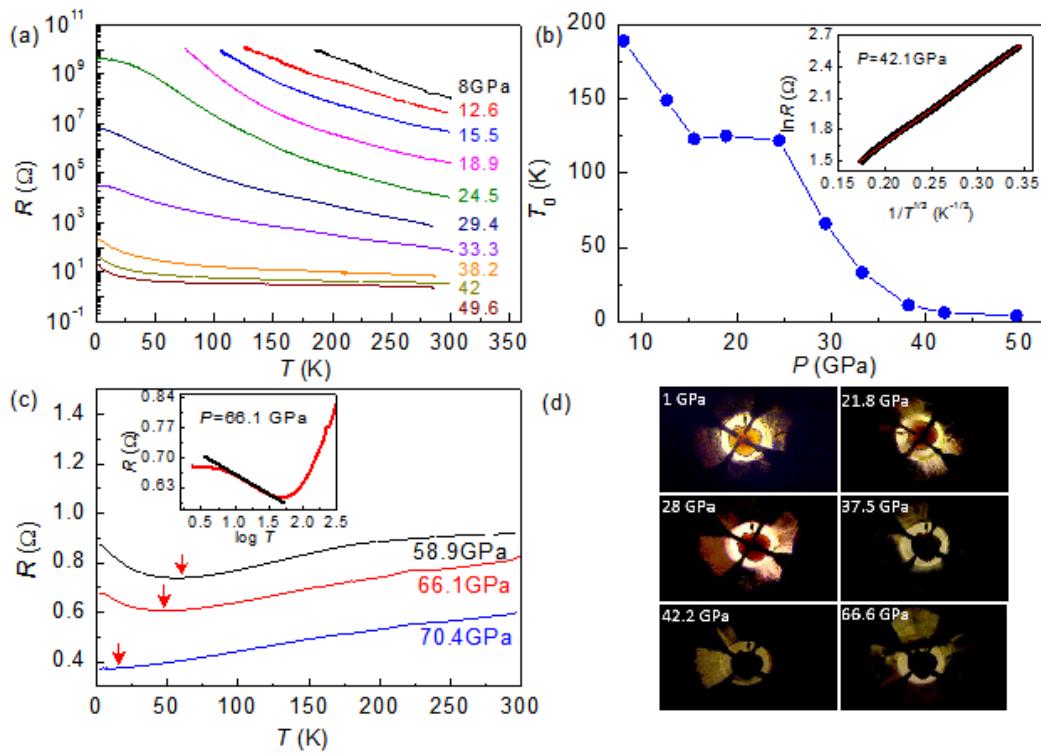


Figure 1. (a) Temperature dependence of resistance $R(T)$ for NaYbSe₂ single crystal in insulating state with pressure up to 49.6 GPa. (b) Pressure dependence of fitted T_0 using variable range hopping model $R(T) = R_0 \exp(T_0/T)^{1/(d+1)}$ ($d = 2$ for the two dimensional property). The inset shows the fitting result at 42 GPa. (c) Temperature dependent resistance $R(T)$ for NaYbSe₂ single crystal between 58.9 GPa and 70.4 GPa. The arrows denote the minimums of $R(T)$ (The temperature at minimum of $R(T)$ is noted as T_{\min}). The inset shows the resistance vs $\log T$ data at 66.1 GPa, showing a linear behavior below T_{\min} (See black line). (d) Piezochromism of the NaYbSe₂ single crystal at various pressures, demonstrating the decrease of band gap with increasing pressure.

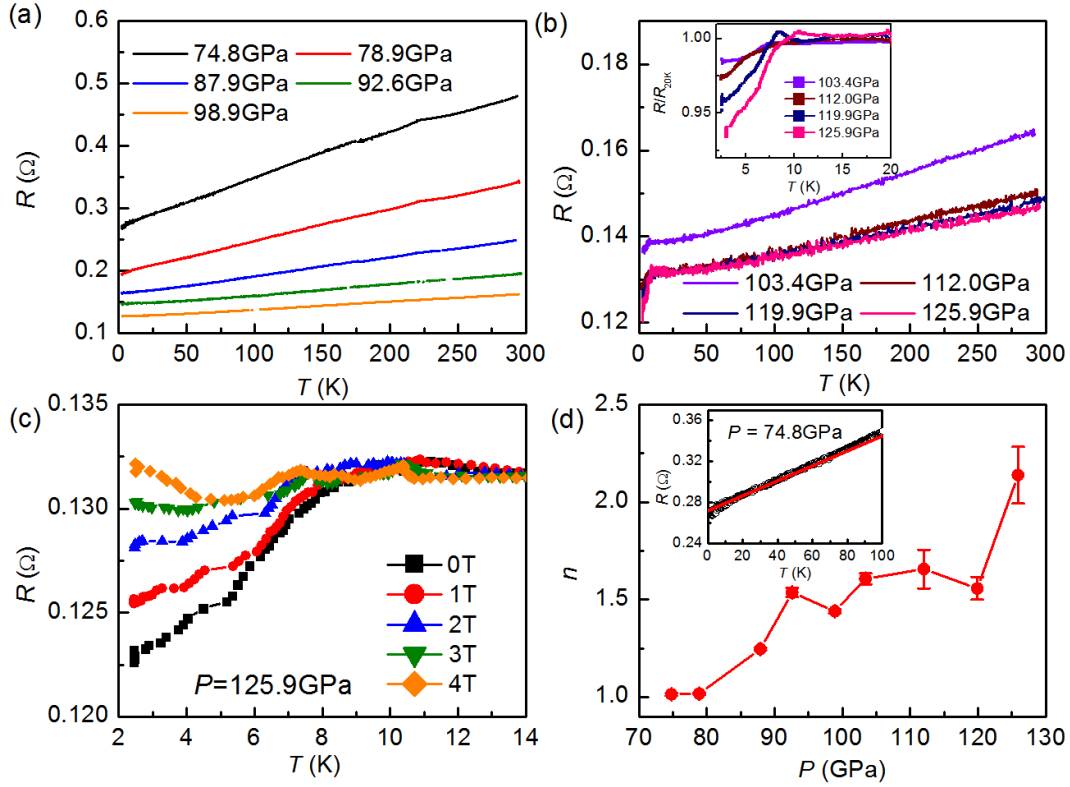


Figure 2. Temperature dependence of $R(T)$ for NaYbSe₂ single crystal in metallic state (a) between 74.8 GPa and 98.9 GPa and (b) between 103.4 GPa to 125.9 GPa. The drop of $R(T)$ in (b) indicates the appearance of superconductivity. The inset of (b) shows the enlarged parts of normalized $R(T)/R(20\text{ K})$ at various pressures. (c) Temperature dependence of $R(T)$ at $P = 125.9$ GPa at different magnetic fields, confirming that the drop of $R(T)$ curve around 8 K is a superconducting transition. (d) Pressure dependence of fitted n in metallic state using the formula $R(T) = R_0 + AT^n$. Inset: experimental and fitting results of $R(T)$ below 100 K at $P = 74.8$ GPa.

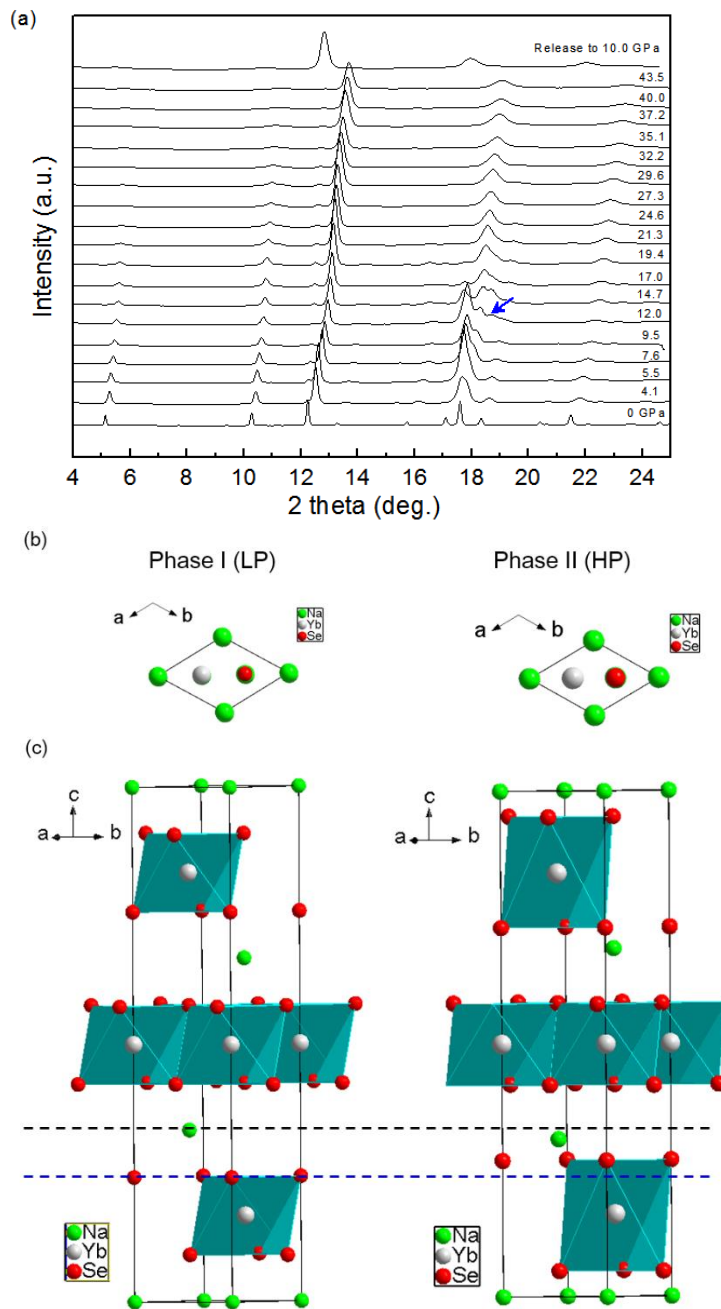


Figure 3. (a) Synchrotron X-ray diffraction patterns of NaYbSe₂ at selected pressures. Additional peaks of new phases are marked by arrow. (b) and (c) Crystal structure of NaYbSe₂ Phase I and II viewed along *c* axis and *ab* plane, respectively.

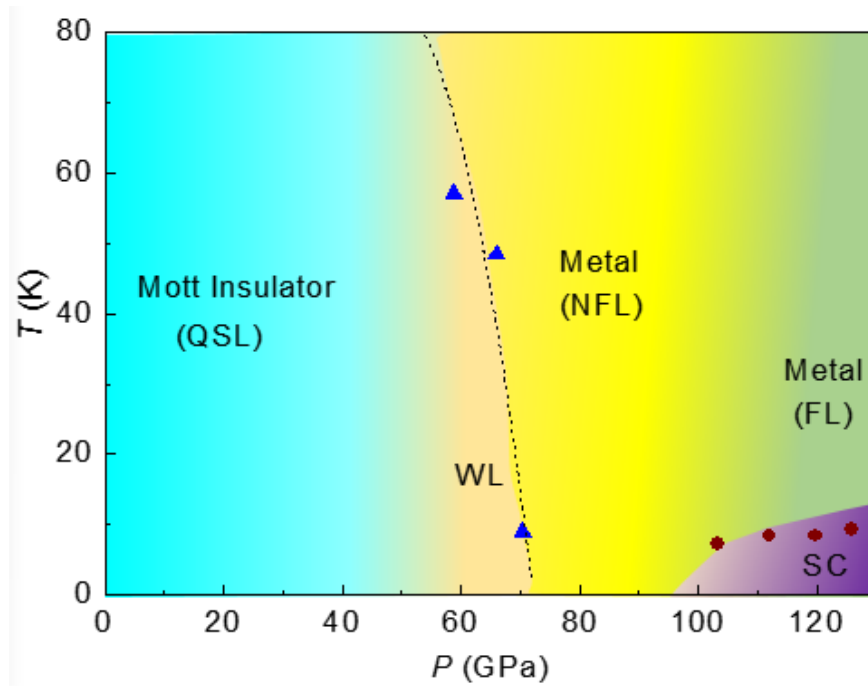


Figure 4. Pressure-temperature (P - T) phase diagram of NaYbSe₂ single crystal. “WL”, “SC”, “QSL”, “FL” and “NFL” are abbreviations for weak localization, superconducting, quantum spin liquid, Fermi liquid and non-Fermi-liquid, respectively. Blue and brown dots denote the phase boundaries of WL-metal and metal-superconductivity.

Supplementary Information

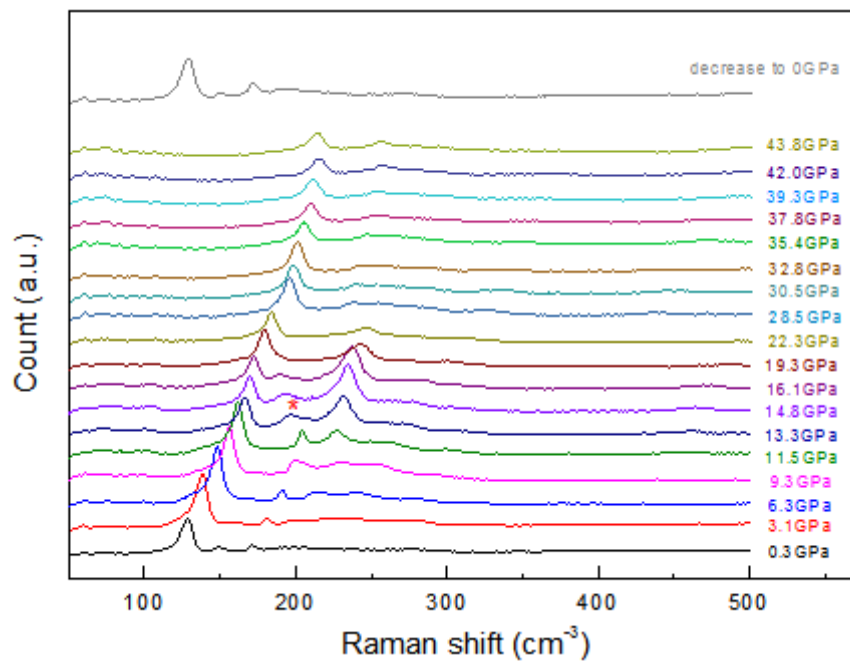


Figure S1. Raman spectrum at selected pressures. The asterisks indicate a new vibration mode.

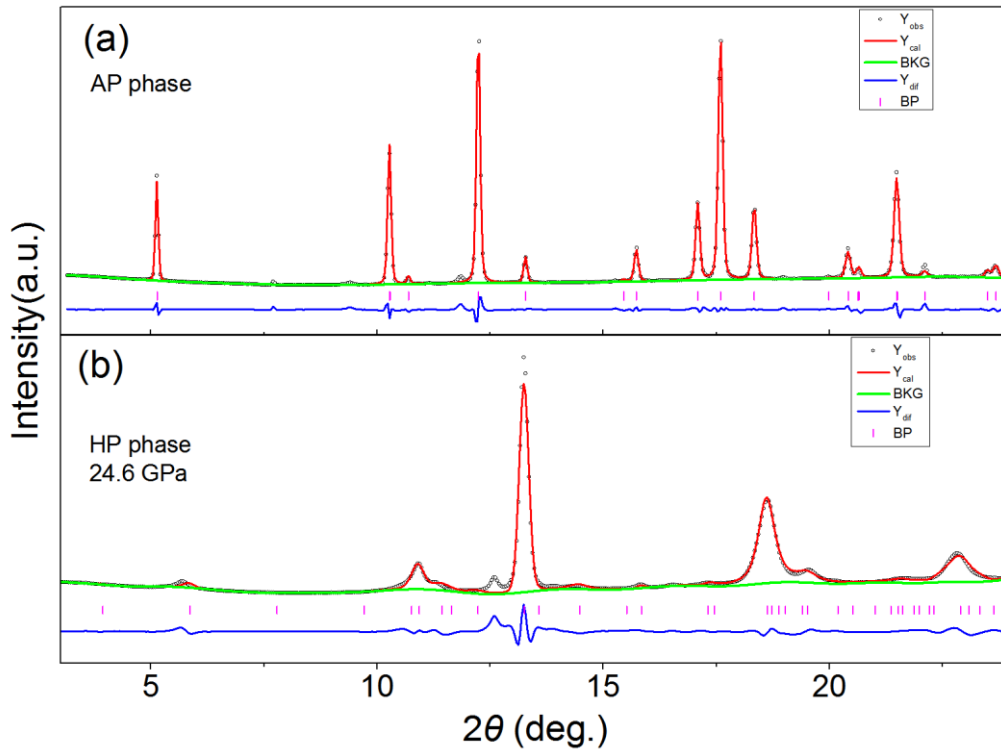


Figure S2. Rietveld refinement of XRD patterns for (a) low pressure phase (phase I, 0 GPa, $R-3mH$) and (b) high pressure phase (phase II, 24.6 GPa, $P-3m1$). Experimental pattern, calculated pattern and their difference shows as black cross, red curve and blue curve, respectively. The pink bars represent the position of Bragg reflections. The wavelength of the X-ray is 0.6199 Å.

Table S1. Refined crystal structural parameters for the low pressure phase (Phase I) and high pressures phase (phase II, 24.6 GPa) data.

	Phase I	Phase II
Space group	<i>R</i> -3 <i>m</i> H	<i>P</i> -3 <i>m</i> 1
<i>a</i> (Å)	4.0536(8)	3.8487(5)
<i>c</i> (Å)	20.7462(4)	18.4729(8)
<i>V</i> (Å ³)	295.23(6)	236.97(7)
Calc. Density (g/cm ³)	5.97(2)	7.44(1)
Na1	(0, 0, 0)	(0, 0, 0)
Na2		(1/3, 2/3, -0.3117)
Yb1	(0, 0, 0.5)	(0, 0, 0.5)
Yb2		(1/3, 2/3, 0.1626)
Se1	(0, 0, 0.2444)	(0, 0, 0.2697)
Se2		(1/3, 2/3, -0.0508)
Se3		(1/3, 2/3, 0.4195)
<i>U</i> _{iso} Na1	0.0151(3)	0.0467(4)
<i>U</i> _{iso} Na2		0.0126(7)
<i>U</i> _{iso} Yb1	0.0016(8)	0.0483(0)
<i>U</i> _{iso} Yb2		0.0142(6)
<i>U</i> _{iso} Se1	0.0021(2)	0.0596(9)
<i>U</i> _{iso} Se2		0.0005(1)
<i>U</i> _{iso} Se3		0.0152(5)
<i>R</i> _{wp} (%)	3.35	4.82
<i>R</i> _p (%)	2.02	2.73